

Cite this: *J. Mater. Chem. A*, 2023, **11**, 12282

Thermodynamic calculation of the ionic conductivity of LiPON glasses and solid electrolytes†

Alberto López-Grande, Glenn C. Mather  and Francisco Muñoz *

LiPON films are one of the most relevant solid electrolytes in Li-ion micro-batteries for low power applications, and the relationships between composition, processing parameters and ionic conductivity have challenged the materials community for the last three decades. Although films have almost exclusively been processed by deposition of Li_3PO_4 polycrystalline pellets, the amorphous nature of LiPON has permitted the study of compositions with glass-forming ability where the effect of improving the conductivity by nitrogen doping is similar. The aim of this work is to form a general model that allows us to calculate the ionic conductivity of LiPON solid electrolytes for whichever composition. The modelling is based on the application of the fundamental laws of chemical equilibrium to elucidate the different chemical species present for each given system composition. For this purpose, a program in the Matlab software was written, capable of solving simultaneous and competitive chemical equilibria. The method, known as the associated solutions model, was applied to the study of the $\text{Li}_2\text{O}-\text{P}_2\text{O}_5$ system, which is the starting point of the present work. The model assumes that the properties of a given glass or amorphous solid, such as the simulated LiPON films, can be obtained as a function of the weighted contributions from each stable compound in the respective composition diagram. Here, $\text{Li}_2\text{PO}_2\text{N}$ oxynitride is used as the main phase and, to validate the computed chemical equilibria, nitridation of crystalline $\text{Li}_4\text{P}_2\text{O}_7$ has been performed by thermal ammonolysis. The combination of the calculations of chemical equilibria together with the structural characterization by XRD and NMR of the products of nitridation from $\text{Li}_4\text{P}_2\text{O}_7$ allowed us to predict both the formation of $\text{Li}_2\text{PO}_2\text{N}$ and the existence of a second oxynitride stoichiometric compound with formula $\text{LiPO}_{1.5}\text{N}$ that would be obtained by nitridation of LiPO_3 . The solution of the system of equilibria was made possible on development of the Gibbs free energy functions of formation of both oxynitride phases, and the calculation of the activation energy and ionic conductivity in either LiPON thin films or oxynitride glasses, offering comparable values to those found in the literature.

Received 8th February 2023
Accepted 24th May 2023

DOI: 10.1039/d3ta00724c

rsc.li/materials-a

1. Introduction

The development of solid-state lithium-ion electrolytes has been an issue of the utmost relevance in the field of energy-storage technologies during recent decades due to the possibility of solving the safety problems related to liquid electrolytes, such as thermal and electrochemical stability, packaging (liquid leakage) and flammability.¹ Among solid electrolytes in use nowadays, amorphous lithium phosphorus oxynitride (LiPON) thin films have been proven as competitive electrolyte materials for micro-power applications due to their chemical stability against the Li metallic anode and the wide electrochemical window *versus* Li/Li^+ (0–5.5 V).² Amorphous LiPON

was firstly produced at Oak Ridge National Laboratory by radio-frequency magnetron sputtering deposition from a Li_3PO_4 target in a N_2 atmosphere.³ The resulting compound, $\text{Li}_{3.3}\text{PO}_{3.9}\text{N}_{0.17}$, showed an ionic conductivity (σ) of $2.2 \times 10^{-6} \text{ S cm}^{-1}$, a factor of 30 greater than that of polycrystalline Li_3PO_4 .³ Numerous subsequent studies by other authors have corroborated the increase in conductivity and the decrease in the activation energy (E_a) of Li diffusion in LiPON thin films under variable conditions of deposition.⁴ However, this observed increase in conductivity on introducing nitrogen in LiPON electrolytes still remains controversial and several hypotheses have been debated.

Based on previous results of oxynitride silicate glasses, Wang *et al.* concluded that the decrease of the electrostatic energy after substitution of P–O for P–N bonds in the amorphous phosphate network results in a decrease in the activation energy of conduction, thus increasing the ionic conductivity.⁵ It was postulated that since N increases the cross-linking density of

Institute of Ceramics and Glass (CSIC), Kelsen 5, 28049 Madrid, Spain. E-mail: fmunoz@icv.csic.es

† Electronic supplementary information (ESI) available. See DOI: <https://doi.org/10.1039/d3ta00724c>



the network through new $-N\equiv$ bonds with neighbouring P atoms, this may favor the formation of (unspecified) conduction pathways for Li diffusion.^{6–8} Actually, both types of nitrogen-to-phosphorus bonds, $-N=$ and $-N\equiv$, are generally found in LiPON thin films, regardless of the method of deposition, and it has been proposed that conductivity is enhanced when the relative content of $-N\equiv$ is higher.⁹ However, recent simulations of LiPON films by Lacivita *et al.* indicated that films with very high lithium contents would present two types of nitrogen atoms, di-coordinated nitrogen N_d ($-N=$) bonded to two phosphorus, and apical nitrogen atoms or N_a ($-N$) bonded to a single phosphorus atom,^{10,11} with the former N_d nitrogen originating the increase of conductivity by nitrogen in LiPON films.

Due to the amorphous character of LiPON electrolytes, another approach that has been used to find a correlation between structure and conduction is through the characterization of lithium phosphorus oxynitride bulk glasses. Lithium-phosphate glasses have a glass-forming range up to nearly 60 mol% Li_2O in the $Li_2O-P_2O_5$ system, corresponding to a LiPON composition of $Li_{1.5}PO_{3.25}$, which is beyond the typical LiPON electrolyte compositions obtained by physical-deposition methods. Nitrogen is instead incorporated into the phosphate glasses by reacting the phosphate melt under a NH_3 flow, giving rise to glasses of general composition $Li_aPO_{b-3x/2}N_x$, according to the substitution of $3O^{2-}$ by $2N^{3-}$.¹² A number of studies have been performed in recent years on the structural modification of the glass network that accompanies nitrogen incorporation and how this influences the increase of ionic conductivity.^{4,5,12–16} One such study indicated that the substitution of oxygen for nitrogen is intimately related to the increase of the relative content of non-bridging oxygens in the glasses. Therein, Mascaraque *et al.* found that the net increase attained in the conductivity for a fixed nitrogen content was lower with increasing lithium content, indicating that the original structure of the given glass composition limits the maximum effect on conductivity.¹⁵

We have recently used a new methodology for modelling the structure and conductivity of $Li_2O-P_2O_5$ glasses,¹⁷ in which the thermodynamic model of associated solutions¹⁸ and the Anderson and Stuart model of ionic conductivity have been employed.¹⁹

The main objective of the present work is to extend such modelling to the study of LiPON compositions, either in the form of glasses or amorphous films. Our starting point is the $Li_2O-P_2O_5-P_3N_5$ system, for which it is necessary to know the stable oxynitride compositions. To date, only one oxynitride with a stoichiometric composition is known, Li_2PO_2N , first predicted and then synthesised and characterised by Senevirathne *et al.*²⁰ This oxynitride phase derives from lithium pyrophosphate $Li_4P_2O_7$ and it was proposed that its structure is built up of $[PO_2N_2]$ tetrahedra, grouped in the form of chains through $P-N=P$ bonds in which all nitrogen atoms are of the N_d type.

We have thus conducted nitridation reactions by ammonolysis in $Li_4P_2O_7$ and Li_3PO_4 to explore the stability domain of Li_2PO_2N and to determine whether another oxynitride phase can be obtained. Subsequently, since the model of associated

solution requires the use of the Gibbs free-energy function of every compound within the composition system of interest, a theoretical derivation of the $G(T)$ of the oxynitride compounds is presented. The work is concluded with modelling of the ionic conductivity for all compositions as a function of both the lithium and nitrogen contents, from which the value for any given oxynitride composition may be predicted.

2. Experimental and methods

2.1. Synthesis and characterization of nitrated phosphates

Lithium pyrophosphate, $Li_4P_2O_7$, and orthophosphate, Li_3PO_4 , were obtained by crystallization of their melts from batches prepared mixing reagent-grade materials Li_2CO_3 (99% ACS. Reagent, Aldrich) and $NH_4H_2PO_4$ (99% ACS. Reagent, Merck) in stoichiometric amounts. The batches were calcined in porcelain crucibles up to 400 °C for 24 h, then melted during 2 h at 950 °C; polycrystalline pyro- and orthophosphate were obtained upon freely cooling the melts. Lithium pyrophosphate was subsequently recrystallized at 550 °C for 24 h to increase its crystallinity.

Nitridation was performed by thermal ammonolysis using a constant NH_3 flow of 0.5 mL min^{-1} on ca. 200 mg of powdered crystalline phosphates. Some samples were sieved under 63 μm to study the influence of the particle size on the reaction. The ammonolysis temperatures varied between 700 °C and 800 °C for $Li_4P_2O_7$ and from 800 °C to 1100 °C for Li_3PO_4 . Steps of heating to the reaction temperature and cooling back to room temperature were performed under a N_2 flow.

Nitrogen content in the samples was determined in a nitrogen/oxygen LECO CHNS-932 elemental instrument by the inert gas fusion method.

X-ray diffraction (XRD) patterns were obtained in Bragg-Brentano geometry using a Bruker D8 Advance diffractometer (Bruker, Germany) equipped with a lynx-eye detector and a germanium monochromator providing monochromatic $Cu K\alpha_1$ radiation ($\lambda = 1.5406 \text{ \AA}$). Diffraction data of powders were collected in the range $10 \leq 2\theta \leq 70^\circ$ using a step width of 0.02° and a step counting time of 1 s.

³¹P magic-angle spinning nuclear magnetic resonance (MAS-NMR) was performed in a Bruker ASX 400 spectrometer at a frequency of 161.96 MHz, using a spinning frequency of 10 kHz in 4 mm rotors. Spectra were acquired with 4 μs pulse length, and a radio-frequency (rf) strength of 60 kHz using recycle delays of up to 3000 s. Chemical-shift values were referred to $(NH_4)_2HPO_4$ at 0.82 ppm with respect to H_3PO_4 (85%).

2.2. Estimation of Gibbs free-energy functions of oxynitride compounds

In the thermodynamic model of associated solutions, a glass can be considered as a solution formed from the glass-oxide components plus the products of their interaction. These products are the so-called salt-like groupings and it is assumed that both their stoichiometry and structure are similar to those of the crystalline compounds that exist in the given system.



Thus, a glass of any composition can be represented by a superposition of various chemical groupings provided the system guarantees the minimum Gibbs energy.¹⁸ The equilibrium molar amount, n , of each salt-like product (j) and unreacted oxide (k) is obtained by solving a set of nonlinear equations composed of the mass balance and mass-action laws of each reaction (j) that takes place in the system:

$$\begin{cases} K_j = \frac{x_j}{\prod_k x_k^{\nu_k^{(j)}}} \\ n_k^0 = n_k + \sum_j \nu_k^{(j)} n_j \end{cases} \quad (1)$$

The stoichiometric coefficients are denoted by the Greek letter ν and the equilibrium constants by the letter K . The superscript 0 denotes the initial molar amount of each unreacted oxide. There are many numerical algorithms capable of efficiently approximating the solution of this system. In this work, the Matlab internal function *fsolve*, which computes a numerical solution of a general nonlinear system of equations, has been used. Some mathematical manipulations of equation system (1) have been performed to facilitate its solution, which are related to the difference of several orders of magnitude between the equilibrium molar amounts of each product. These manipulations have been detailed in a previous work.¹⁷

In the case of LiPON compositions, in either glass or amorphous thin-film form, Li_2O , P_2O_5 and P_3N_5 were chosen as the reactants to simulate the system in chemical equilibrium. Thus, the system of reactions to be solved is composed of the reactions of formation of the three lithium phosphates, LiPO_3 , $\text{Li}_4\text{P}_2\text{O}_7$ and Li_3PO_4 , plus those of formation of the lithium oxynitride phosphates to be identified below.

The value of the Gibbs free-energy function of each compound is required to calculate the equilibrium constant of the corresponding formation reaction, $K = \exp(-G/RT)$. The Gibbs functions of meta, pyro and orthophosphate compounds to be used herein are the same as those employed in the solution of the system published in ref. 17; however, the G functions of the oxynitride compounds are unknown, so a method of estimation is required. Any derivation of G must involve calculation of enthalpy and entropy contributions.

The core of the present approach is the Gibbs-Helmholtz equation from which, if $H(T)$ is known, it is possible to find the $G(T)$ function as given below:

$$\frac{\partial}{\partial T} \left(\frac{G}{T} \right)_{p,x_i} = -\frac{H}{T^2} \quad (2)$$

The procedure for integration of $G(T)$ is the following: for a small interval of T , H can be considered as a constant. Thus, by integration of eqn (2) from T_1 to T_2 (any two temperatures close enough to consider H as constant) the following relation is obtained:

$$\frac{G(T_2)}{T_2} - \frac{G(T_1)}{T_1} = H \left(\frac{1}{T_2} - \frac{1}{T_1} \right) \quad (3)$$

If we work with small steps of temperature, $G(T_{i+1})$ can be obtained from the previous value $G(T_i)$, and the initial value ($i = 1$) corresponding to $T = 298$ K:

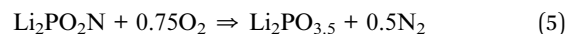
$$\left\{ G(T_{i+1}) = T_{i+1} \left[H(T_i) \left(\frac{1}{T_{i+1}} - \frac{1}{T_i} \right) + \frac{G(T_i)}{T_i} \right] \right. \quad (4a)$$

$$\left. \{ G(T_1) = G_r^0 = H_r^0 - T_0 S_r^0 \right\} \quad (4b)$$

To use this procedure, the $H(T)$ function and the S_r^0 value of the oxynitride compounds should be estimated.

Tessier *et al.* studied the enthalpy of formation of oxynitride phosphate glasses and obtained a general expression for the standard formation enthalpy against the nitrogen content in oxynitride glasses by comparing the difference in bond energy with the oxidation reaction.²¹ The known $H(T)$ of the corresponding phosphate composition is employed, assuming that $H(T)$ for the oxynitride is the value of $H(T)$ of the phosphate phase coupled with the change in the bond energies on substituting oxygen for nitrogen. Thus, herein the values of the bond energies of O–O, N–N, P–N and P–O are used, as well as the value of the enthalpies of formation of the lithium phosphate compounds from which the oxynitrides are to be obtained.

Considering the oxidation reaction of the $\text{Li}_2\text{PO}_2\text{N}$ oxynitride to form $\text{Li}_4\text{P}_2\text{O}_7$:



the enthalpy of oxidation can be calculated from the change in binding energies:

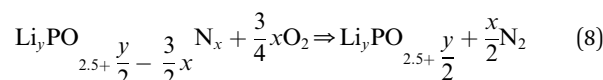
$$E_{\text{ox}}^0 = 0.5E_{\text{N-N}}^0 + (3.5 - 2)E_{\text{P-O}}^0 - E_{\text{P-N}}^0 - 0.75E_{\text{O-O}}^0 \quad (6)$$

In the case of the oxidation of $\text{Li}_2\text{PO}_2\text{N}$ to pyrophosphate, the reaction enthalpy is -380.53 ± 3.67 kJ mol⁻¹, so the enthalpy of the nitridation reaction will be the same.

The enthalpy of formation of pyrophosphate must then be added to this enthalpy of reaction to obtain the enthalpy of formation of the oxynitride:

$$H_f^0(\text{LiPON}) = H_f^0(\text{LiPO}) + (E_{\text{ox}}^0) \quad (7)$$

This method can be generalised for any lithium and nitrogen contents through the following general oxidation reaction:

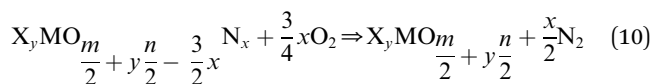


In this case, the enthalpy of oxidation is:

$$E_{\text{ox}}^0 = \frac{x}{2}E_{\text{N-N}}^0 + \frac{3}{2}xE_{\text{P-O}}^0 - xE_{\text{P-N}}^0 - \frac{3}{4}xE_{\text{O-O}}^0 \quad (9)$$



As seen from eqn (9), the change in $H(T)$ does not depend on the amount of lithium present in the compound. The reaction described in eqn (8) can be generalised to any nitridation reaction from a given phosphate composition, irrespective of the type of cation X of charge n or the central atom of the oxide anion M of charge m :



$$E^0 = \frac{x}{2} E_{N-N}^0 + \frac{3}{2} x E_{M-O}^0 - x E_{M-N}^0 - \frac{3}{4} x E_{O-O}^0 \quad (11)$$

Finally, the difference in bond energy can be calculated using the following approximation:²²

$$\Delta E = \Delta E^0 + \frac{3}{2} R(T - T_0)$$

Hence, the function of enthalpy against temperature can be obtained for the given oxynitride.

The standard entropy of formation employed in eqn (6) is derived using Latimer's method,²³ which establishes that the entropy of a crystalline solid can be calculated by adding the contributions of the cation and the anion from which it is formed. As stated in the aforementioned article, the entropy of a solid compound is a function of the masses of the constituent atoms and of the forces acting between these atoms: the greater the mass and the lower the force, the greater the entropy.

In accordance with the above, the entropy of an ionic solid depends on the magnitude of the ionic charges. To illustrate this, Latimer calculated the contribution of the chloride ion in combination with +1, +2 and +3 ions by subtracting the entropy of the cations from the experimental salt entropy value, assuming the entropy of the cations equal to that of their corresponding elements, estimated previously.²⁴ The agreement in entropy values of Cl^- calculated for the three types of salt (Cl^- plus cation +1, Cl^- plus cation +2 and Cl^- plus cation +3) was remarkable. A close examination of the data for a large number of anions showed that a similar loading effect existed in all cases.

Consequently, Latimer proposed to arbitrarily assign all the variation of the entropy with the charge to the negative ion and to tabulate said entropy as a function of the charge of the cation from the experimental values. The entropy of the salt is then calculated as the sum of the entropy of the monatomic cation and that of the corresponding anion.

For example, for the compound $Ag_2SO_4 = 2Ag + SO_4^{2-}$, the entropies tabulated by Latimer are 12.8 cal per mol per °C for the element Ag and 22.0, 17.2, 13.7 and 12 cal per mol per °C for SO_4^{2-} , depending on whether it is attached to a cation with a +1, +2, +3 or +4 charge, respectively. In this case, the Ag^+ ion has a +1 charge, thus the value of the entropy of SO_4^{2-} for the calculation is 22.0 cal per mol per °C. The entropy of Ag_2SO_4 will therefore be $S_f^0 = (2 \times 12.8 + 22.0)$ cal per mol per °C = 47.6 cal per mol per °C. The experimental value is 47.8 cal per mol per °C.

The problem with this method is that several measurements are needed for each type of anion to be able to tabulate the average entropy as a function of the charge of the cation. Hence, for compounds in which the entropy of their anion has not been measured, it is not possible to use this method, as is the case for the PO_3^- anion.

To solve this problem, it is necessary to return to the initial statement made in Latimer's article:²³ "the entropy of a solid compound is a function of the masses of the constituent atoms and of the forces acting between these atoms: the greater the mass and the smaller the force, the greater the entropy". Therefore, to estimate the entropy of the unknown anions, an attempt has been made to establish a relationship of the type $S_f^0 \propto \text{mass} \times 1/(\text{interaction forces})$ from the data of known anions,^{23,25} which are tabulated in Table S1.† Using Latimer's method, the unknown entropy of other anions has also been calculated from entropy data of different salts.²⁶ These entropies are tabulated in Table S2.†

To quantify the effect of mass, the molecular mass of the anion will be taken as a variable. To quantify the interaction forces, the binding energy central atom – secondary atom (P–O for PO_4^{3-} , Si–F for SiF_6^{3-} ...) will be used. This correlation has been established in the present work for oxide anions, and it can be extrapolated to LiPON (PO_xN_y anions) for two reasons: first, the amount of nitrogen in these compounds is very low in comparison with the amount of oxygen; second, only a rough estimate of entropy is needed to start the procedure, as will be seen in the results section. The bond energy in PO_xN_y anions to use the entropy correlation of oxides can be estimated as

$$B_e = B_e(P-O) \frac{x_O}{x_O + x_N} + B_e(P-N) \frac{x_N}{x_O + x_N} \quad (12)$$

The correlation between entropy, molecular weight and binding energy can be seen in Fig. S1 of the ESI† file, where experimental data for the entropy of anions have also been plotted.

The binding energy shows the highest correlation with the entropy, and the most precise expression found so far to estimate the entropy through the molecular weight (M_m) and the binding energy (B_e) is the following:

$$\sqrt{S_f^0} = A + B \times \ln \left(\frac{1000 \times M_m}{B_e} \right) \quad (13)$$

where the entropy is expressed in $J \text{ mol}^{-1} \text{ K}^{-1}$, the molecular mass in g mol^{-1} and the binding energy in kJ mol^{-1} . Using these units for oxides, $A = 0.757815094$ and $B = 1.62345464$; the strength of the correlation is $R^2 = 69.01\%$ (Fig. S2†).

From the estimation of the standard entropy (eqn (13)) and the enthalpy (eqn (7) and (8)), $G(T)$ has been calculated for the oxynitride compounds, $LiPO_{1.5}N$ and Li_2PO_2N as will be seen below, by using eqn (4). Fig. S3 to S5 of ESI† show a comparison of the calculated Gibbs free energy functions using the above method and the experimental ones, as obtained from the FactSage database, where a very good agreement can be seen. On the other hand, Fig. S6† expresses the calculated G functions for the two oxynitride phases that will be used in the calculations below.



2.3. Calculation of ionic conductivity

The ionic conductivity (σ) is calculated as a function of temperature (T) from the following Arrhenius equation, which assumes that a glass is a weak electrolyte:²⁷

$$\sigma T = n \frac{e^2 \lambda^2 \nu_0}{6K_B} \exp\left(-\frac{E_a}{K_B T}\right) \quad (14)$$

where n is the total cation concentration (Li^+ in this case), e is the fundamental charge, λ is the jump distance between cation sites, ν_0 is the jump attempt frequency, E_a is the activation energy and K_B is Boltzmann's constant. Charge-carrier concentration, n , can readily be calculated subsequently once the relative content of each phase in the system is known, considering the stoichiometric number of Li in each phase, as shown previously.¹⁷ Assuming isotropy (as stated in the aforementioned paragraph), the average jump distance, λ , can then be calculated from the charge-carrier concentration as $\lambda = \sqrt[3]{1/n}$. Hopping frequency has been taken from far-infrared studies of Exharhos *et al.* as reported earlier.¹⁷

The activation energy can be calculated through the Anderson & Stuart model as described in ref. 17. One can approximate the electrostatic contribution (binding energy) by using Coulomb's law for one ion pair with the addition of a covalence parameter γ . Anderson and Stuart justified the introduction of this parameter by claiming that, in the materials that they studied, the direct use of Coulomb's law led to excessive activation-energy values due to the fact that the electron cloud of O^{2-} anions is rather easily deformed by the cation, lowering the binding energy.¹⁹ Coulomb's law must, therefore, be modified to take this into account as follows:

$$E_a = \frac{1}{\gamma} Z_{\text{Li}^+} Z_{\text{O}^{2-}} \left(\frac{1}{R_{\text{Li}^+} + R_{\text{O}^{2-}}} - \frac{2}{\lambda} \right) \quad (15)$$

where R_{Li^+} and $R_{\text{O}^{2-}}$ are the ionic radii of lithium and oxygen atoms, 1.4 Å and 0.6 Å, respectively. According to their experiments, Anderson and Stuart concluded that the covalence parameter can be approximated by the dielectric constant.^{17,19} However, a review conducted by the authors of the present work has brought to light that γ is, in fact, equivalent to the dielectric constant. The reason for this confusion is that the authors used the CGS system in their work, so the constant term in Coulomb's law equals 1. However, this is only true in a pure vacuum. In this case, $\epsilon_r = 1$, and in the CGS system we have:

$$\frac{1}{4\pi\epsilon} = \frac{1}{4\pi\epsilon_0} = 1 \frac{\text{statC}}{\text{cm}}$$

Nevertheless, for a dielectric material such as glass, ϵ_r has to be considered, and eqn (15) becomes:

$$\begin{aligned} E_a &= \frac{Z_{\text{Li}^+} Z_{\text{O}^{2-}}}{\epsilon_r} \left(\frac{1}{R_{\text{Li}^+} + R_{\text{O}^{2-}}} - \frac{2}{\lambda} \right) [\text{CGS}] \\ &= \frac{Z_{\text{Li}^+} Z_{\text{O}^{2-}}}{4\pi\epsilon_0\epsilon_r} \left(\frac{1}{R_{\text{Li}^+} + R_{\text{O}^{2-}}} - \frac{2}{\lambda} \right) [\text{IS}] \end{aligned} \quad (16)$$

For lithium phosphate glasses, a value of $\epsilon_r = 10$ can be taken as an approximation.^{28,29} Hence, to evaluate the influence of N on the dielectric behavior of the material, a 10% increase of the dielectric constant for each 10% wt. of N added into the composition can be considered as a first approximation, considering data of dielectric constants in alkali- and alkaline-earth-containing oxynitride silicate glasses.³⁰ The dielectric constant for $\text{Li}_2\text{PO}_2\text{N}$ would thus reach a value of 11.5. It should be remarked that even if 10 is only an approximation of the dielectric constant for $\text{Li}_4\text{P}_2\text{O}_7$, this may not be that relevant since what we seek is the effect on E_a and σ due to the increase of the dielectric constant while introducing N with respect to the value of the oxide composition. However, taking a value of 10 for the dielectric constant has worked well in the previous work on the calculation of ionic conductivity in lithium phosphate glasses.¹⁷ The strain-energy contribution to the activation energy can be neglected due to the small size of the Li^+ cation.¹¹

Finally, to determine n and λ for eqn (14), the molar volume (V_m) of the material is required, and can be calculated from the equation of state of the SVTD model:¹⁹

$$G = n_i g_i + RT \sum n_i \log(x_i) \quad (17)$$

where g_i are the Gibbs free energies of the phases of the system's phase diagram. From eqn (17), molar volume can be obtained as:

$$V_m = \left(\frac{\partial G}{\partial p} \right)_T = \sum n_i V_{mi} \quad (18)$$

where V_{mi} are the molar volumes of the phases. With the exception of $\text{LiPO}_{1.5}\text{N}$, most values can be taken from experimental data.^{26,31,32} For $\text{LiPO}_{1.5}\text{N}$, Korotkov's method can be used to estimate the molar volume on establishing a relationship between certain metric properties of the material and the macroscopic density:³³

$$\rho = \frac{1.661kM_m}{\sum l_i V_i} \quad (19)$$

where k is a "filling factor" that accounts for the fraction of the total space occupied by the atoms of the phase; l_i and V_i are, respectively, the stoichiometric number and the volume of each atom.

The filling factor typically drops in the range 0.4–0.6 for inorganic compounds, so a value of 0.5 is usually taken as an average. However, lithium phosphorus oxynitride compounds have two elements in their structure (Li and N) which contract the network, so this number is expected to be higher than usual and may be estimated from volume experimental data of the oxynitride $\text{Li}_2\text{PO}_2\text{N}$, 229.47 Å³ according to Senevirathne *et al.*²⁰ Knowing V_m (ref. 20) and M_m , we can use eqn (19) to calculate the filling factor, which gives $k = 0.66$. Using this value as a first estimate for lithium phosphorus oxynitride compounds and eqn (19) again, we obtain $V_m(\text{LiPO}_{1.5}\text{N}) = 28.46 \text{ cm}^3 \text{ mol}^{-1}$, which is, as expected, below the value of 34.62 cm³ mol⁻¹ of LiPO_3 , the phosphate from which $\text{LiPO}_{1.5}\text{N}$ is formed.



3. Results and discussion

3.1. Nitrogen incorporation in lithium phosphates, $\text{Li}_4\text{P}_2\text{O}_7$ and Li_3PO_4

Fig. 1 shows the results of the ammonolysis reactions on lithium pyrophosphate plotted as wt% N against temperature for samples without and with sieving below $63\ \mu\text{m}$ (1a), reaction time (1b) and the number of consecutive reactions for temperatures between $700\ ^\circ\text{C}$ and $800\ ^\circ\text{C}$, each for a reaction time of 3 h (1c).

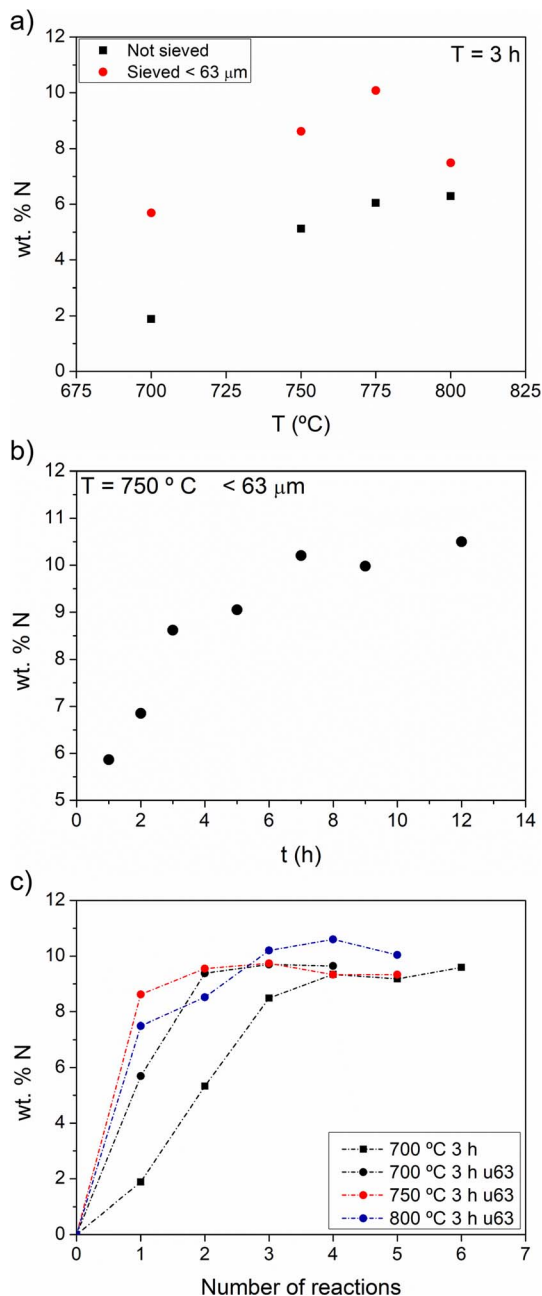


Fig. 1 Nitrogen introduced in $\text{Li}_4\text{P}_2\text{O}_7$ by thermal ammonolysis as a function of (a) temperature, (b) time of reaction and (c) number of consecutive reactions.

Fig. 1a shows that particle size has a marked influence on the amount of N that can be introduced after a single treatment of 3 h, particularly below $800\ ^\circ\text{C}$. This strong dependence on particle size results from the solid-gas reaction, in which the available surface area of the solid reactant is a crucial variable. Furthermore, higher temperatures give rise to a higher content of nitrogen for the first 3 h of ammonolysis, while at $800\ ^\circ\text{C}$ the effect is reversed, likely due to the faster sintering of the powdered solid that reduces the surface area in contact with NH_3 .

The plateau for reaction times up to 12 h at $750\ ^\circ\text{C}$ (Fig. 1b) indicates that there is a limit to the content of nitrogen that can be reached. As in Fig. 1a, the maximum content that can be reached in these conditions is *ca.* 10 wt%. Fig. 1c shows the content of N analyzed in samples submitted to consecutive reactions of 3 h at $750\ ^\circ\text{C}$; samples were re-ground after each reaction to study the newly introduced nitrogen into de-agglomerated samples. Even if the temperature is increased to $800\ ^\circ\text{C}$ or the number of reaction steps increases, the maximum N content in the samples lies between 10 and 11 wt%.

Fig. 2a shows the XRD patterns of $\text{Li}_4\text{P}_2\text{O}_7$ and some of the nitrated products for increasing nitrogen contents, from bottom to top: 0 wt% N ($\text{Li}_4\text{P}_2\text{O}_7$), 2.82 wt% ($700\ ^\circ\text{C}$, 2 h), 5.86 wt% ($750\ ^\circ\text{C}$, 3 h), 8.62 wt% ($750\ ^\circ\text{C}$, 3 h) and 10.08 wt% ($775\ ^\circ\text{C}$, 3 h), all submitted to a single reaction step.

The samples with 2.82 and 5.86 wt% N are mainly composed of $\text{Li}_4\text{P}_2\text{O}_7$ (ICSD59243) and minor amounts of $\gamma\text{-Li}_3\text{PO}_4$ (ICSD79427). The presence of $\gamma\text{-Li}_3\text{PO}_4$ reflections increases for higher nitrogen contents while the intensities of $\text{Li}_4\text{P}_2\text{O}_7$ reflections decrease. Either very minor or no presence of $\text{Li}_4\text{P}_2\text{O}_7$ is observed for 8.62 and 10.08 wt% N samples, in accordance with the computational results of the chemical equilibria to be discussed later in this section. From the XRD patterns in Fig. 2a, it is concluded that only crystalline phases of $\text{Li}_4\text{P}_2\text{O}_7$ and Li_3PO_4 are present and that nitrogen should enter into an amorphous phase.

Fig. 2b, however, exhibits the XRD patterns of the nitrated products obtained for two nitrogen contents, 4.34 and 7.98 wt%, that were submitted to ammonolysis reactions at $675\ ^\circ\text{C}$ for 6.5 h and at $750\ ^\circ\text{C}$ for 3 h after 3 consecutive reactions, respectively, and which reveal the crystallisation of additional phases, particularly that of $\text{Li}_2\text{PO}_2\text{N}$ (ICSD188493). Some additional reflections are observed at 13.2° and 26.5° , which could not be identified with known phases in the ICSD and NIST databases. For $\text{Li}_2\text{PO}_2\text{N}$, we note that although the *d*-spacings of its principal peaks match those of the XRD pattern published by Senevirathne *et al.*²⁰ the intensities do not match to the same extent, which may indicate some compositional variation or preferred orientation.

According to the computational results of $\text{Li}_2\text{O-P}_2\text{O}_5\text{-P}_3\text{N}_5$ equilibria, there should not be any reflections of $\text{Li}_2\text{PO}_2\text{N}$ below ~ 7.3 wt% N. The $\text{Li}_2\text{PO}_2\text{N}$ peaks observed in the pattern with 4.34 wt% N may arise from nitridation of the $\gamma\text{-Li}_3\text{PO}_4$ phase that forms on nitriding $\text{Li}_4\text{P}_2\text{O}_7$, in accordance with computational results that predict the decomposition of $\gamma\text{-Li}_3\text{PO}_4$ into $\text{Li}_2\text{PO}_2\text{N}$ and Li_2O with increasing N content. We speculate that



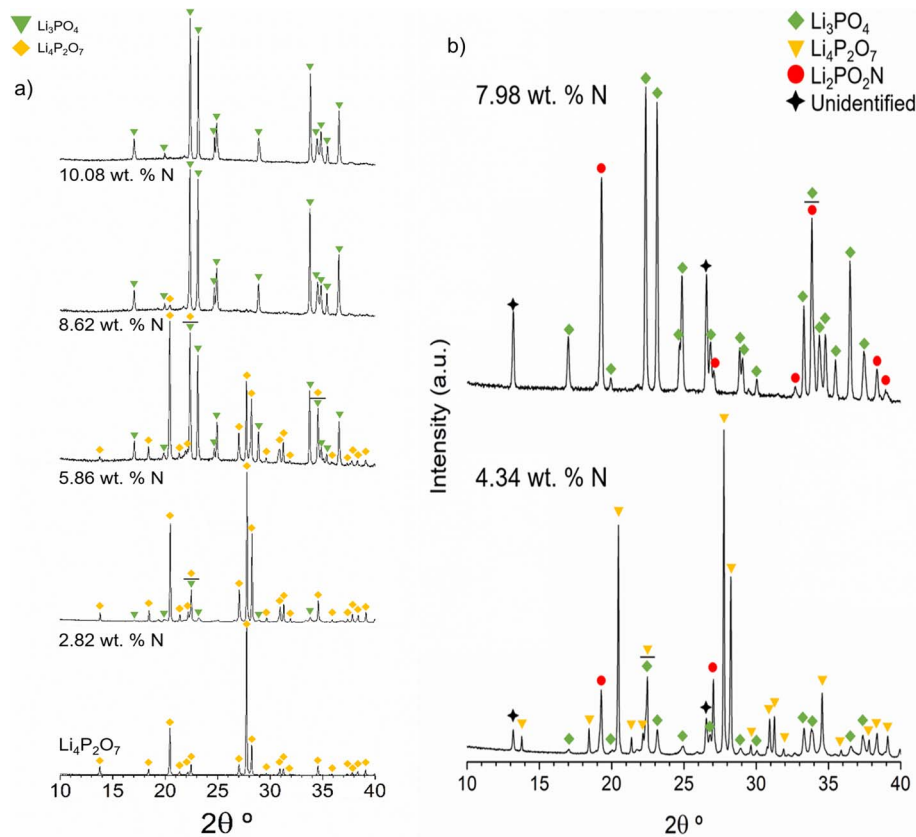


Fig. 2 XRD patterns of nitrated $\text{Li}_4\text{P}_2\text{O}_7$ as a function of nitrogen content for (a) several single-step reactions and (b) samples that exhibit partial crystallization of oxynitrides, either due to increased reaction time or after undergoing consecutive reactions.

the additional unidentified reflections may be attributable to a $\text{LiPO}_{1.5}\text{N}$ phase predicted to form by computational results of chemical equilibria, as shown below.

Fig. 3a shows the ^{31}P MAS NMR spectra of two samples with nitrogen contents of 5.86 and 10.08 wt% N, as obtained by nitridation at 750 °C for 1 h and 775 °C for 3 h, respectively. The sample with 5.86 wt% N shows two very intense and narrow resonances at -3.9 and -6.2 ppm with Lorentzian profiles, which are attributable to the two crystallographic sites of phosphorus in $\text{Li}_4\text{P}_2\text{O}_7$. The spectrum also shows an even more intense peak at 9.45 ppm, attributed to Li_3PO_4 phase detected in the XRD patterns (Fig. 2), together with a very broad resonance resembling an amorphous background that may be ascribed to the presence of phosphorus in an amorphous phase. For the second sample with *ca.* 10 wt% N, the broad resonance with a large chemical-shift distribution and the peak attributed to Li_3PO_4 again appears, but the peaks typical of $\text{Li}_4\text{P}_2\text{O}_7$ are absent.

Fig. 3b shows the ^{31}P NMR spectra of the samples with 4.34 and 7.98 wt% of nitrogen prepared with longer ammonolysis treatment in a single reaction at 675 °C for 6.5 h and for the sample after three consecutive reactions at 750 °C for 3 h each, respectively. The sample of lowest nitrogen content clearly shows the two resonances of $\text{Li}_4\text{P}_2\text{O}_7$ (-3.9 and -6.1 ppm) and that of Li_3PO_4 (9.45 ppm); however, four more signals with Lorentzian profile are also present at 4.74, 10.79, 11.94 and

14.42 ppm, indicating the presence of further phosphorus atoms in one or more crystalline environments. The sample of nitrogen content 7.98 wt% shows the same resonances as those of the 4.34 wt% N sample, except for those of $\text{Li}_4\text{P}_2\text{O}_7$. Both simulations include a broad Gaussian resonance at *ca.* 0 and 2 ppm arising from phosphorus in an amorphous phase that had not yet crystallised after the given reactions. Marple *et al.* have very recently performed *ab initio* calculations of the chemical-shift tensor of ^{31}P for a number of oxynitride and nitride compounds and reported a value of 14.949 ppm for the isotropic chemical shift of ^{31}P in $\text{Li}_2\text{PO}_2\text{N}$,³⁴ which has a single phosphorus crystallographic site.²⁰ Given that the calculated value of chemical shift would not be precisely the experimental one of ^{31}P in $\text{Li}_2\text{PO}_2\text{N}$, it is reasonable to suppose that the resonance at 14.4 ppm in the NMR spectra of Fig. 3b is attributable to $\text{Li}_2\text{PO}_2\text{N}$, in agreement with the presence of reflections of $\text{Li}_2\text{PO}_2\text{N}$ in the XRD pattern of the same sample (Fig. 3a). The three other resonances at *ca.* 4, 10 and 11 ppm may thus correspond to the unidentified crystalline phase appearing in both XRD patterns.

The crystalline phases identified by XRD and NMR for the different N contents suggest that the first reaction to consider during nitridation is the simultaneous decomposition of pyrophosphate into ortho- and metaphosphate phases, with the latter undergoing the partial substitution of oxygen for nitrogen:



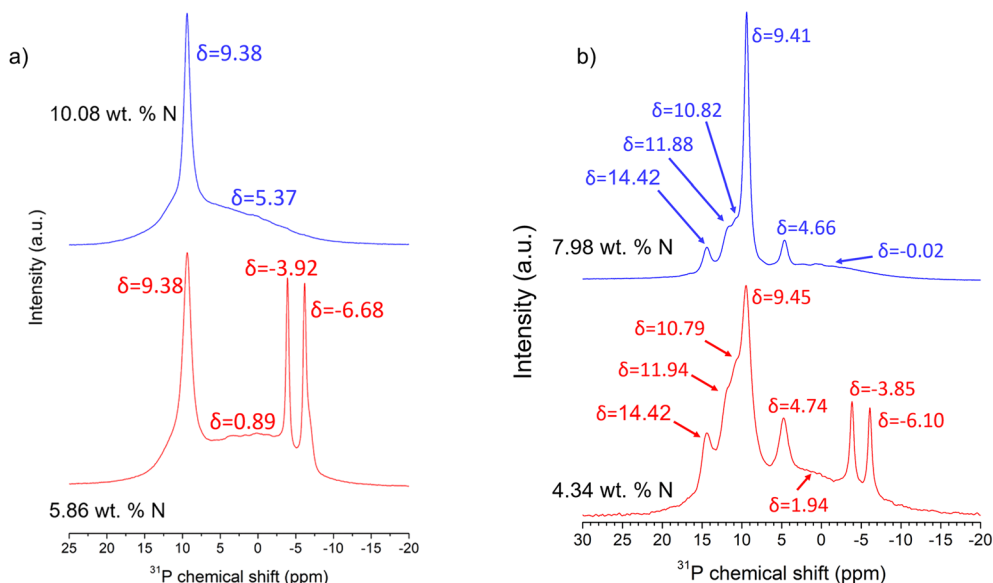


Fig. 3 ^{31}P MAS NMR spectra of two nitrated $\text{Li}_4\text{P}_2\text{O}_7$ compositions prepared by (a) single step reaction at 750 °C for 1 h (5.86 wt% N) and 775 °C for 3 h (10.08 wt% N) and (b) two nitrated $\text{Li}_4\text{P}_2\text{O}_7$ compositions prepared by single reaction at 675 °C for 6.5 h (4.34 wt% N) and 3 consecutive reactions at 750 °C for 3 h (7.98 wt% N).



The maximum incorporation of nitrogen into the LiPO_3 structure would be obtained for the stoichiometry $\text{LiPO}_{1.5}\text{N}$, in which every phosphorus atom is bonded to two nitrogen atoms *via* P–N=P bonds, as in the structure of its homologous phase for Li/P = 2 ($\text{Li}_2\text{PO}_2\text{N}$),²⁰ and where all tetrahedral building units are of the type $[\text{PO}_2\text{N}_2]$. This would correspond to the stoichiometry of a metaphosphate glass where the maximum nitrogen content of 18.4 wt% is attained. However, considering the decomposition of the pyrophosphate into Li_3PO_4 and the nitrated metaphosphate amorphous phase, the nitrogen content where the reaction stops corresponds to only 7.3 wt%. Above this, the XRD patterns do not show evidence of $\text{Li}_4\text{P}_2\text{O}_7$; therefore, as the reaction still proceeds up to the maximum observed N content of *ca.* 10% (Fig. 1), the formation of a second oxynitride phase should be considered. This phase appears to be closely related to $\text{Li}_2\text{PO}_2\text{N}$, which is the nitrated product of $\text{Li}_4\text{P}_2\text{O}_7$ for 15.4 wt% nitrogen content. In fact, if the known oxynitride $\text{Li}_2\text{PO}_2\text{N}$ is considered as a new reaction product, the calculated nitrogen content that corresponds to an equimolar system composed of the sum of Li_3PO_4 , $\text{LiPO}_{1.5}\text{N}$ and $\text{Li}_2\text{PO}_2\text{N}$ is 9.9 wt%. This value closely approximates the maximum obtained in the nitridation experiments (Fig. 1).

Nitridation of Li_3PO_4 has also been carried out to examine the formation of $\text{Li}_2\text{PO}_2\text{N}$. Fig. 4 shows the XRD patterns of a set of nitrated samples for increasing nitrogen contents, all of which exhibit reflections of Li_3PO_4 .

For the highest nitrogen contents, reflections attributable to $\text{Li}_2\text{PO}_2\text{N}$ phase are clearly visible. This suggests that Li_3PO_4 decomposes to Li_2O and a nitrated amorphous phase from which crystallization of $\text{Li}_2\text{PO}_2\text{N}$ takes place. As will be shown

below from thermodynamic calculations, this oxynitride phase is consistent with the presence of $\text{Li}_2\text{PO}_2\text{N}$.

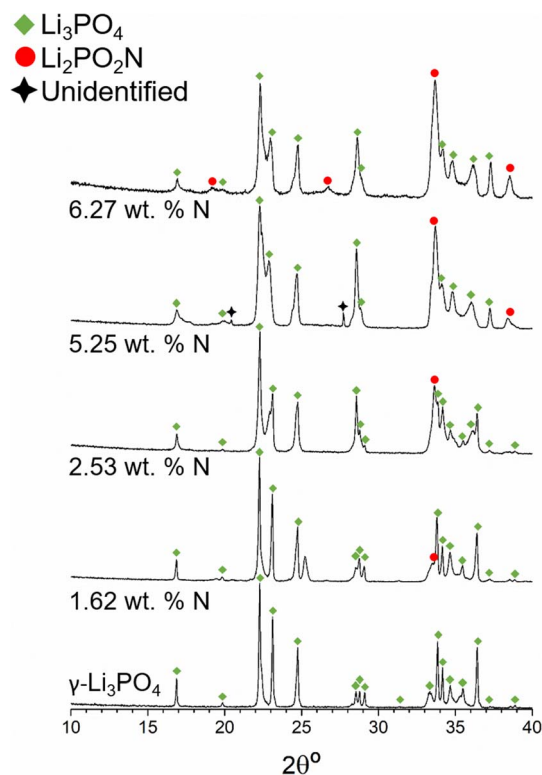


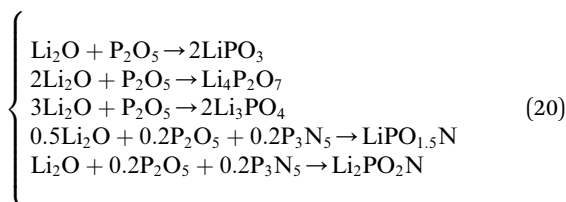
Fig. 4 XRD patterns of nitrated Li_3PO_4 as a function of nitrogen content from 0 to 6.27 wt% N.



Li_2O is not observed in the XRD patterns, which could be due to the very small amount formed and because Li_2O can simultaneously react with water forming $\text{Li}(\text{OH})$ of high volatility.

3.2. Thermodynamic modelling of oxynitride systems

As discussed above, the system of compositions under consideration is $\text{Li}_2\text{O}-\text{P}_2\text{O}_5-\text{P}_3\text{N}_5$. The reactions of formation to be considered are those that give rise to the three lithium-phosphate phases, LiPO_3 , $\text{Li}_4\text{P}_2\text{O}_7$ and Li_3PO_4 , which were considered in the modelling of the $\text{Li}_2\text{O}-\text{P}_2\text{O}_5$ glass system,¹⁷ and the reactions that form the two oxynitride phases derived from the proposed nitridation reactions above, $\text{LiPO}_{1.5}\text{N}$ and $\text{Li}_2\text{PO}_2\text{N}$:



The system of nonlinear equations is given by the constants of equilibrium of each reaction of formation and the mass balances of each of the reacting compounds:

$$\left\{ \begin{array}{l} K_{\text{LP}} = \frac{x_{\text{LP}}}{x_{\text{Li}_2\text{O}} \times x_{\text{P}_2\text{O}_5}} \\ K_{\text{L}_2\text{P}} = \frac{x_{\text{L}_2\text{P}}}{x_{\text{Li}_2\text{O}}^2 \times x_{\text{P}_2\text{O}_5}} \\ K_{\text{L}_3\text{P}} = \frac{x_{\text{L}_3\text{P}}}{x_{\text{Li}_2\text{O}}^3 \times x_{\text{P}_2\text{O}_5}} \\ K_{\text{L}_2\text{PN}} = \frac{x_{\text{L}_2\text{PN}}}{x_{\text{Li}_2\text{O}} \times x_{\text{P}_2\text{O}_5}^{0.2} \times x_{\text{P}_3\text{N}_5}^{0.2}} \\ K_{\text{LPN}} = \frac{x_{\text{LPN}}}{x_{\text{Li}_2\text{O}}^{0.5} \times x_{\text{P}_2\text{O}_5}^{0.2} \times x_{\text{P}_3\text{N}_5}^{0.2}} \\ n_{\text{Li}_2\text{O}}^0 = n_{\text{Li}_2\text{O}} - (n_{\text{LP}} + 2n_{\text{L}_2\text{P}} + 3n_{\text{L}_3\text{P}} + 0.5n_{\text{L}_2\text{PN}} + n_{\text{L}_2\text{PN}}) \\ n_{\text{P}_2\text{O}_5}^0 = n_{\text{P}_2\text{O}_5} - (n_{\text{LP}} + n_{\text{L}_2\text{P}} + n_{\text{L}_3\text{P}} + 0.2n_{\text{L}_2\text{PN}} + 0.2n_{\text{L}_2\text{PN}}) \\ n_{\text{P}_3\text{N}_5}^0 = n_{\text{P}_3\text{N}_5} - (0.2n_{\text{L}_2\text{PN}} + 0.2n_{\text{L}_2\text{PN}}) \end{array} \right. \quad (21)$$

The system consists of 8 equations and 8 variables, each n_i , given that each x_i may be written as $x_i = n_i / \sum n$.

Fig. 5 shows the solution of the chemical equilibria for the reaction of nitridation of $\text{Li}_4\text{P}_2\text{O}_7$ in two possible situations: (i) nitridation only produces the $\text{Li}_2\text{PO}_2\text{N}$ oxynitride (Fig. 5a); (ii) nitridation results in the formation of both $\text{LiPO}_{1.5}\text{N}$ and $\text{Li}_2\text{PO}_2\text{N}$ oxynitrides (Fig. 5b).

In the first case, a very minor amount of Li_3PO_4 would appear, which tends to disappear concomitantly with increasing oxynitride content during the course of the reaction; this scenario is not observed experimentally. In the second situation, the $\text{LiPO}_{1.5}\text{N}$ oxynitride and Li_3PO_4 are both formed in similar amounts up to $x = 0.2$, corresponding to ~ 7.3 wt% N, above which point no $\text{Li}_4\text{P}_2\text{O}_7$ remains. With greater N content,

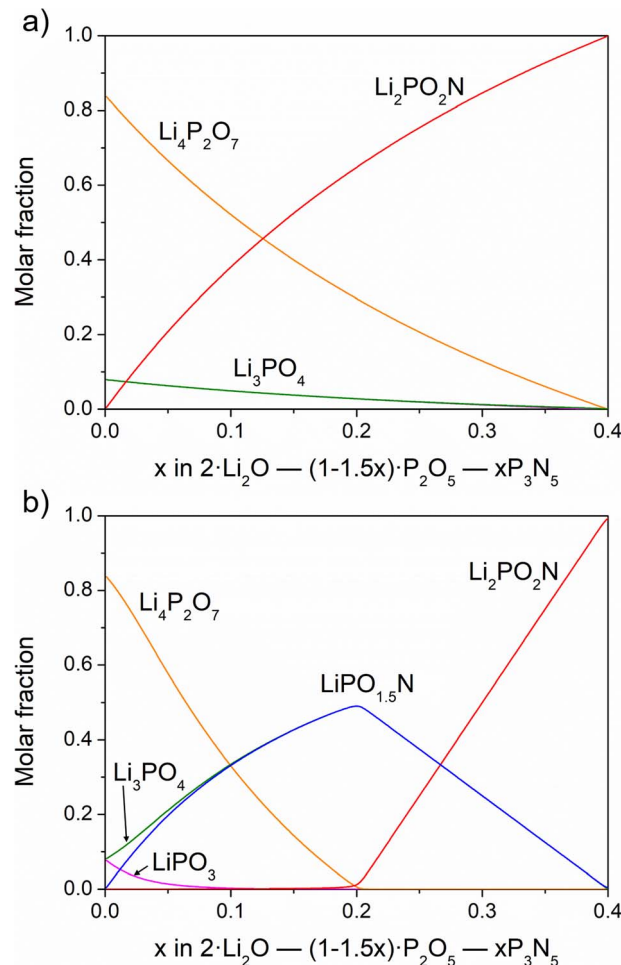
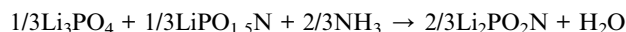
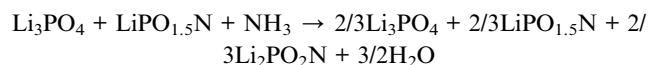


Fig. 5 Results of solved chemical equilibria for $\text{Li}/\text{P} = 2$ as a function of nitrogen content (a) considering $\text{Li}_2\text{PO}_2\text{N}$ only as a reaction product and (b) considering $\text{LiPO}_{1.5}\text{N}$ and $\text{Li}_2\text{PO}_2\text{N}$ as reaction products.

the concentrations of both $\text{LiPO}_{1.5}\text{N}$ and Li_3PO_4 decrease and $\text{Li}_2\text{PO}_2\text{N}$ instead forms. When the nitrogen content reaches *ca.* 10 wt%, $x = 0.27$, there are, in fact, equimolar amounts of Li_3PO_4 and the two oxynitrides, as proposed above. Therefore, after the formation of 1 mol of Li_3PO_4 and $\text{LiPO}_{1.5}\text{N}$ from $\text{Li}_4\text{P}_2\text{O}_7$, the reaction for the formation of $\text{Li}_2\text{PO}_2\text{N}$ above $x = 0.2$ is as follows:



This reaction proceeds until $x = 0.27$ where Li_3PO_4 , $\text{LiPO}_{1.5}\text{N}$ and $\text{Li}_2\text{PO}_2\text{N}$ are in equal proportions:



The solution of chemical equilibria confirms, therefore, that the equimolar sum of Li_3PO_4 and the two oxynitrides accounts for a 9.9 wt% of N, as observed in the nitridation from pyrophosphate. When the number of mols of Li_3PO_4 and $\text{LiPO}_{1.5}\text{N}$



are smaller than that of $\text{Li}_2\text{PO}_2\text{N}$ formed at 9.9 wt% N, the reaction between Li_3PO_4 and $\text{LiPO}_{1.5}\text{N}$ becomes increasingly slower and the formation of further $\text{Li}_2\text{PO}_2\text{N}$ much more difficult. This explains why it is not possible to increase the nitrogen content further than ~ 10 to 11 wt%.

The simulations of the ^{31}P NMR spectra of the samples with 5.86 and 10.08 wt% N in Fig. 3 were performed with the *Dmfit* analysis software.³⁵ The quantification of NMR spectra of Fig. 3a gives orthophosphate and amorphous phase, corresponding to $\text{LiPO}_{1.5}\text{N}$ and $\text{Li}_2\text{PO}_2\text{N}$, with very similar values to those obtained in the estimated contents of the calculated proportions in Fig. 5b. The value of wt% N calculated from x in the system, according to the quantification of the different phases, gives 5.4% ($x = 0.15$) and 10.4% N ($x = 0.28$), in reasonable agreement with the analysed nitrogen contents of these samples, thereby confirming the validity of the proposed reaction scheme. On the other hand, the NMR spectra shown in Fig. 3b confirm the two scenarios resulting from calculations: (i) for the 4.34 wt% N sample, $\text{Li}_4\text{P}_2\text{O}_7$ is still present together with Li_3PO_4 , in addition to the four resonances attributed to $\text{Li}_2\text{PO}_2\text{N}$ and another crystallised phase; (ii) the sample with 7.98 wt% N only shows the resonance of Li_3PO_4 and those of crystallised oxynitrides as observed in the corresponding XRD pattern. The presence of $\text{Li}_4\text{P}_2\text{O}_7$ or Li_3PO_4 phases for the nitrogen contents 4.34 and 7.98 wt% (Fig. 3b) is thus supported by the calculated equilibria. The only point of difference between calculated and experimental results is that for 4.34% N (Fig. 5b) there is crystallisation of $\text{Li}_2\text{PO}_2\text{N}$ seen by XRD (Fig. 2b) and NMR (Fig. 3b). This may be explained if part of the Li_3PO_4 that originates from decomposition of $\text{Li}_4\text{P}_2\text{O}_7$ simultaneously reacts with NH_3 to produce $\text{Li}_2\text{PO}_2\text{N}$. As discussed below, modelling of the nitridation reaction of Li_3PO_4 indeed produces the $\text{Li}_2\text{PO}_2\text{N}$ oxynitride.

Fig. 6a shows the solution of the chemical equilibria at the Li_2O content of the metaphosphate line against the nitrogen content. The results clearly indicate the formation of the $\text{LiPO}_{1.5}\text{N}$ oxynitride phase in parallel with a decrease in the content of LiPO_3 .

The nitridation reaction that takes place in this case would be:



We note that the above reaction is exactly that which should proceed from the nitridation of a lithium metaphosphate melt and which would continue until all the LiPO_3 is converted into the respective oxynitride, $\text{LiPO}_{1.5}\text{N}$, corresponding to a N content of 18.4 wt%. To conclude, we postulate that the formation of an oxynitride of formula $\text{LiPO}_{1.5}\text{N}$ is coherent both experimentally and theoretically with the above proposed nitridation reactions. Nevertheless, a phase of a stoichiometry with Li/P and $\text{N}/\text{P} = 1$ is predicted to exist in the equilibrium phase diagram of the $\text{Li}_2\text{O}-\text{P}_2\text{O}_5-\text{P}_3\text{N}_5$ system. Further work is underway with the aim of synthesising the pure $\text{LiPO}_{1.5}\text{N}$ phase, which is expected to form

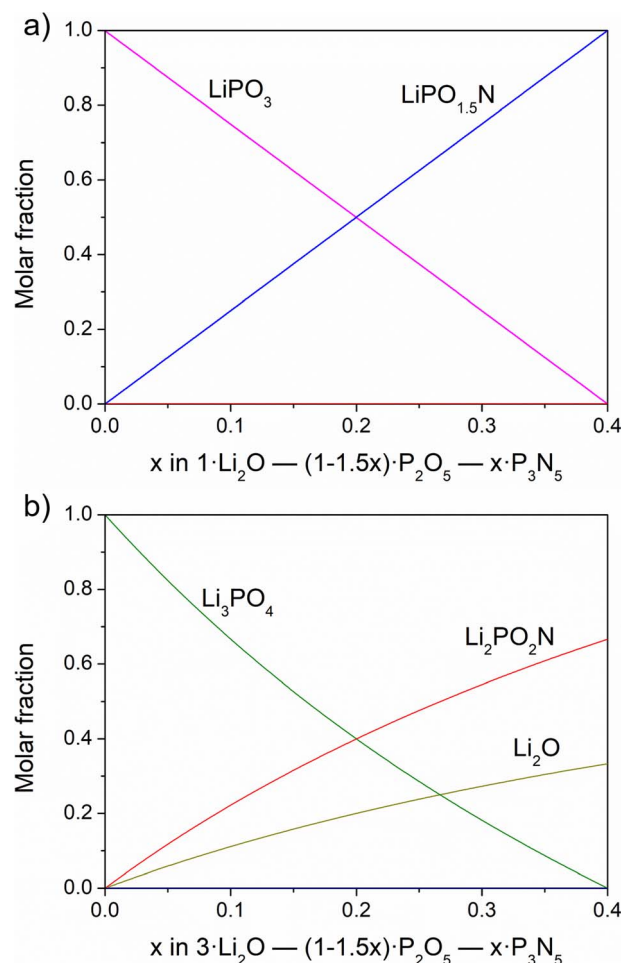


Fig. 6 Results of solved chemical equilibria for (a) $\text{Li}/\text{P} = 1$ and (b) $\text{Li}/\text{P} = 3$ as a function of nitrogen content.

from the nitridation of LiPO_3 . We have not been able to provide experimental details on the formation of $\text{LiPO}_{1.5}\text{N}$ as a pure phase, as we were not able to isolate it from the nitridation products of $\text{Li}_4\text{P}_2\text{O}_7$, nor did we obtain conclusive results from the direct nitridation of LiPO_3 . We attempted to nitride the LiPO_3 metaphosphate in different ways to synthesise phase-pure $\text{LiPO}_{1.5}\text{N}$; however, at this point, we have not observed conclusive proof of its synthesis. The nitridation of lithium metaphosphate *via* a similar route as that employed for the pyrophosphate $\text{Li}_4\text{P}_2\text{O}_7$ presents the inconvenience that its melting temperature is much lower, only 656 °C, and the formation of only a small amount of liquid phase during the reaction considerably limits nitrogen incorporation because the surface area is very much reduced, giving rise to products of very low nitrogen content.

The solution of the system if nitridation proceeds from Li_3PO_4 is represented in Fig. 6b. In this case, nitridation involves reaction of Li_3PO_4 and NH_3 with simultaneous formation of the $\text{Li}_2\text{PO}_2\text{N}$ phase and Li_2O :



Therefore, we have no need to consider any other oxynitride phase apart from $\text{LiPO}_{1.5}\text{N}$ and $\text{Li}_2\text{PO}_2\text{N}$, and we believe that, due to structural reasons, the formation of a similar oxynitride to these two phases from Li_3PO_4 would not be plausible. A stable structure made up of $[\text{PO}_2\text{N}_2]$ tetrahedra linked through $\text{P}-\text{N}=\text{P}$ bonds, as in the two former oxynitrides, would have an excess of oxygens per phosphorus and an unbalanced charge. It appears, therefore, that Li_3PO_4 decomposes into Li_2O and the stable $\text{Li}_2\text{PO}_2\text{N}$ phase on the substitution of oxygen for nitrogen.

3.3. Ionic conductivity of LiPON glasses and amorphous films

Fig. 7a displays \log_{10} of electrical conductivity (σ) calculated at 298 K vs. the nitrogen content, as represented by x in the system $n\text{Li}_2\text{O}-(1-1.5x)-\text{P}_2\text{O}_5-x\text{P}_3\text{N}_5$, for the lines of composition of $n = 1, 2, 3$, representing LiPO_3 , $\text{Li}_4\text{P}_2\text{O}_7$ and Li_3PO_4 , respectively; Fig. 7b shows the corresponding activation energy of conduction in eV as a function of x .

The first point to note is that, whereas the conductivity calculated for the non-nitrided compositions ($x = 0$) increases

from LiPO_3 to $\text{Li}_4\text{P}_2\text{O}_7$ and Li_3PO_4 , in agreement with the expected variation of conductivity in $\text{Li}_2\text{O}-\text{P}_2\text{O}_5$ glasses as a function of Li_2O ,¹⁷ the degree of increase from metaphosphate to pyrophosphate is notably higher than that from pyrophosphate to orthophosphate. This indicates that the mobility of Li^+ in the orthophosphate is smaller with respect to that in the other phases.

Previous studies of lithium-ion conductivity in single crystals and polycrystalline lithium pyro- and orthophosphates documented conductivity values that are, in general, much lower for Li_3PO_4 than for $\text{Li}_4\text{P}_2\text{O}_7$. Voronin *et al.* reported conductivity values of the order of $10^{-3} \text{ S cm}^{-1}$ at 720 K (447 °C),³⁶ and Ivanov-Shitz *et al.* have reported conductivity values in single crystals of $\gamma\text{-Li}_3\text{PO}_4$ in the range $2-4 \times 10^{-5} \text{ S cm}^{-1}$ at 450 °C, while Hu *et al.*³⁷ and Huggins *et al.*³⁸ also presented a conductivity of $3 \times 10^{-5} \text{ S cm}^{-1}$, significantly lower than the conductivity of $\text{Li}_4\text{P}_2\text{O}_7$ at a similar temperature. The calculated conductivities of the $\text{Li}_4\text{P}_2\text{O}_7$ and Li_3PO_4 compositions presented here, Fig. 7a, correspond to the amorphous solids so the most valid comparison is with the corresponding amorphous thin films; nevertheless, the relationship with the conductivity observed in crystalline ceramics is indicative that the orthophosphate composition presents a somewhat lower conductivity than that expected. The great majority of research on LiPON thin films involves processing by deposition of Li_3PO_4 targets, so it is not readily possible to make a direct comparison with values of the films made up of $\text{Li}_4\text{P}_2\text{O}_7$ specifically.

The conductivity for the metaphosphate compositions, in which $\text{LiPO}_{1.5}\text{N}$ forms by nitridation of LiPO_3 , exhibit a linear increase with increasing nitrogen content. This is consistent with an enhanced mobility of Li^+ ions in $\text{LiPO}_{1.5}\text{N}$, such that a linear increase of the conductivity of the system occurs proportional to the linear increase of the molar fraction of $\text{LiPO}_{1.5}\text{N}$, as observed in Fig. 7a. On the other hand, the conductivity of the nitrided systems obtained from $\text{Li}_4\text{P}_2\text{O}_7$ ($n = 2$) and Li_3PO_4 ($n = 3$) show slightly different behavior, with some deviation from linearity to a smaller slope occurring at the highest nitrogen contents. This change of trend is more marked for Li_3PO_4 than for $\text{Li}_4\text{P}_2\text{O}_7$, where the conductivity difference of the former between $x = 0.4$ and $x = 0$ is of about an order of magnitude, 30% less than the increment calculated in the metaphosphate line. The curves of activation energy against nitrogen content (Fig. 7b) decrease their slope with increasing x , in agreement with experimental results in both glasses and LiPON thin films.

Literature results, notably those by Mascaraque *et al.* for oxynitride lithium phosphate glasses within a range of $\text{Li}_2\text{O}/\text{P}_2\text{O}_5$ ratios,¹⁵ showed a regular increase of conductivity with increasing nitrogen content, although with some dispersion in the data. This scattering may be because of heterogeneities in the bulk glass samples, which result in different behavior from that predicted in the present calculations. The values of $\log_{10} \sigma$ at 298 K are also in good agreement with experimental results for the compositions for which bulk glasses can be prepared:¹⁴⁻¹⁶ both experimental and calculated values are in the range $\log_{10} \sigma = -8.5$ to -6.5 in S cm^{-1} , the conductivity increasing with higher lithium and nitrogen contents.

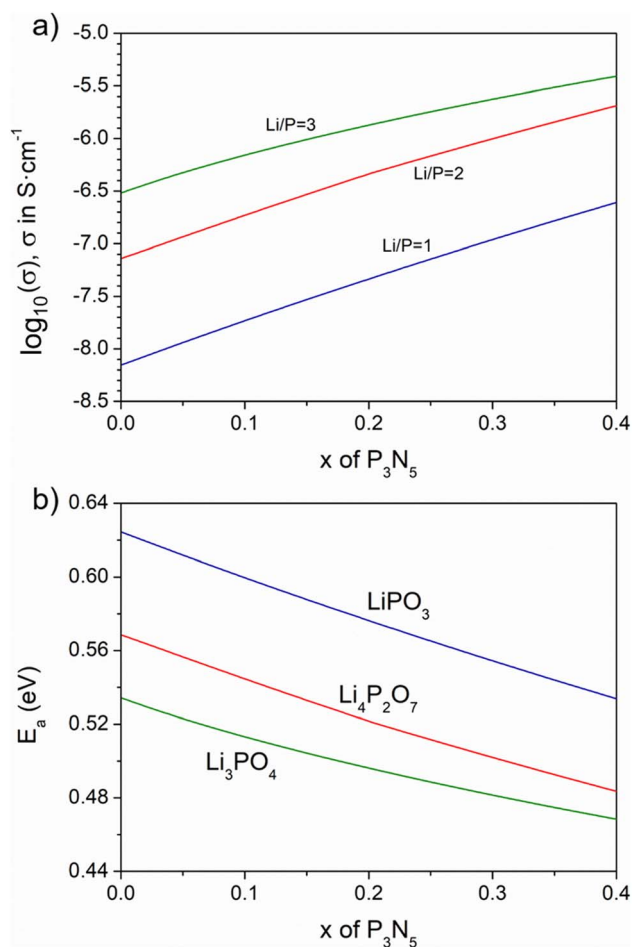


Fig. 7 Calculated ionic conductivity (a) and activation energy (b) at 25 °C for Li/P = 1, 2 and 3 nitrided compositions as a function of nitrogen content.



Furthermore, some representative experimental values of the ionic conductivity in LiPON thin films obtained by deposition of Li_3PO_4 have been compared with the values calculated in the present work in Table 1. It can be seen that calculated and experimental values are in good agreement.

Fig. 8a shows the electrical conductivity against the Li/P ratio for nitrogen contents in the range $x = 0-0.40$. All conductivity curves in Fig. 8a exhibit an increase with both lithium and nitrogen; however, besides the smaller value of conductivity for Li_3PO_4 as a function of lithium than that expected from a linear increase, the observed difference in the conductivity between $x = 0.10$ and 0.40 is clearly smaller at the $n = 3$ line than at $n = 1$. This difference has been plotted for each nitrogen content as a function of the Li/P ratio in Fig. 8b. For the lowest nitrogen content ($x = 0.1$), $\Delta\log_{10}$ is almost constant at 0.4 for all Li/P values. With higher nitrogen content, $\Delta\log_{10}$ becomes more significant but decreases as the lithium content increases. At the highest nitrogen content of $x = 0.4$, the conductivity difference between the nitrated compositions is clearly higher at the metaphosphate line, with formation of $\text{LiPO}_{1.5}\text{N}$, than for the orthophosphate one ($\text{Li}_2\text{PO}_2\text{N} + \text{Li}_2\text{O}$). This means that the improvement of conductivity that can be attained through formation of the $\text{LiPO}_{1.5}\text{N}$ oxynitride phase can be as high as that obtained at any other lithium content.

One of the key observations in the work by Mascaraque *et al.* was that, in LiPON glasses,¹⁵ the higher the lithium content, the smaller the augmentation of conductivity for a constant nitrogen. The authors pointed out that the ratio between the bridging oxygen atoms (BO) to non-bridging oxygens (NBO) in the network influences the degree of augmentation of the conductivity after nitrogen incorporation. In oxynitride glasses, the BO/NBO ratio decreases for increasing nitrogen contents as $-\text{N}\equiv$ and $-\text{N}=\text{}$ bonds are formed and substitute for both BOs and NBOs. According to the substitution rules first established by Marchand,³⁹ more BOs will be substituted than NBOs and so the BO/NBO decreases upon nitridation. Part of the NBOs are also substituted, but considering that there are two types of NBOs, $\text{P}=\text{O}$ and $\text{P}-\text{O}-\text{Li}$, the number of NBOs of the $\text{P}-\text{O}-\text{Li}$ type would be constant and the $\text{P}=\text{O}$ type mainly substituted so that charge neutrality is maintained. Lithium ions are coordinated by several non-bridging oxygens of $[\text{PO}_4]$ tetrahedral units

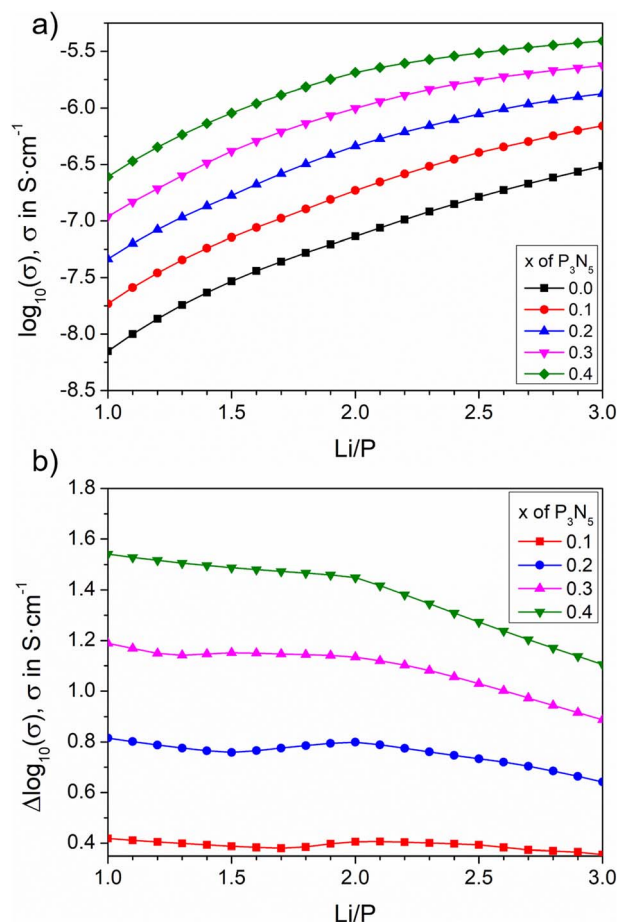


Fig. 8 Calculated ionic conductivity and its increment as a function of Li/P ratio for selected nitrogen contents.

with a typical coordination number between 4 and 5 in lithium-phosphate glasses,⁴⁰ so if the relative number of negatively charged non-bridging oxygens increases, the mobility of lithium ions would be enhanced, increasing conductivity. The authors demonstrated that the smallest increments in conductivity were found for the smallest changes in the BO/NBO ratio,¹⁵ which is corroborated in the present calculations.

The number density of Li^+ ions (n_{Li^+}) is plotted in Fig. 9 as a function of the Li/P ratio and nitrogen contents in the range $x = 0.00-0.40$.

The curve for the density of lithium ions in the oxide compositions ($x = 0$) shows a near-linear behaviour, although it exhibits a slight curvature with a smaller slope near the orthophosphate line ($n = 3$). However, the non-linearity of the curves increases with greater nitrogen content. For compositions with Li/P ratios below 2, the increase of n_{Li^+} becomes steeper with nitrogen content with the greatest difference observed for the n_{Li^+} of the respective non-nitrated composition at Li/P = 2. When Li/P approaches 3, the number density of lithium even decreases with respect to the non-nitrated compositions.

Below 0.2 of Li/P, nitridation of any composition in the $\text{LiPO}_3\text{-Li}_4\text{P}_2\text{O}_7$ region will mainly produce $\text{LiPO}_{1.5}\text{N}$, and only $\text{Li}_2\text{PO}_2\text{N}$ from $\text{Li}_4\text{P}_2\text{O}_7$ (Li/P = 2) at the highest nitrogen

Table 1 Comparison of ionic conductivity and activation energy of calculated and experimental values of LiPON thin-films

Li/P ratio (ref.)	x^a	$\log_{10} \sigma$ at 298 K, exp	E_a exp. (eV)	$\log_{10} \sigma$ at 298 K, calc.	E_a calc. (eV)
2.900 (ref. 13)	0.18	-5.48	0.540	-6.21	0.515
2.410 (ref. 20)	0.37	-6.21	0.499	-5.65	0.482
2.795 (ref. 20)	0.30	-6.12	0.551	-5.77	0.489
2.708 (ref. 20)	0.17	-6.54	0.551	-6.38	0.525
2.854 (ref. 20)	0.16	-6.68	0.594	-6.34	0.522
2.637 (ref. 22)	0.13	-6.05	N/A	-6.68	0.541
2.140 (ref. 23)	0.36	-6.00	0.530	-5.79	0.489

^a x in $n\text{Li}_2\text{O}-(1-1.5x)-\text{P}_2\text{O}_5-x\text{P}_3\text{N}_5$.



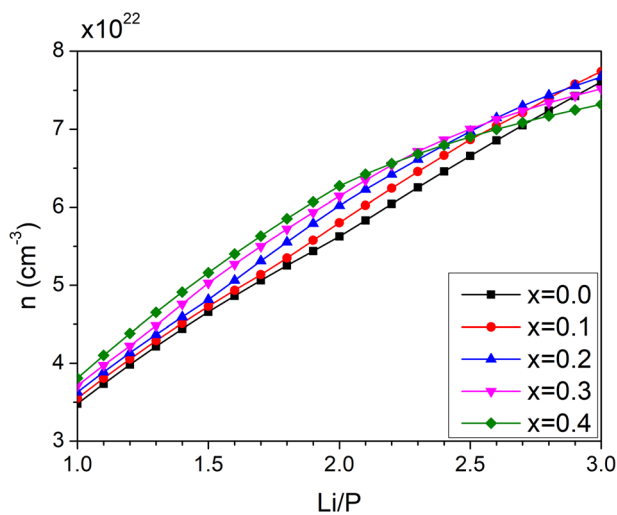


Fig. 9 Calculated concentration of total charge carriers as a function of Li/P ratio for nitrogen contents between $x = 0.1$ and 0.4 .

contents. On the other hand, nitridation above $\text{Li/P} = 2$, in the system $\text{Li}_4\text{P}_2\text{O}_7\text{-Li}_3\text{PO}_4$, will give rise to $\text{Li}_2\text{PO}_2\text{N}$ only. There is, therefore, a notable difference in the increase in number density depending on the oxynitride that is formed and thus, its contribution to the improvement of the ionic conductivity becomes remarkably different. The calculated values of n_{Li^+} in $\text{LiPO}_{1.5}\text{N}$ and $\text{Li}_2\text{PO}_2\text{N}$ are 3.81×10^{22} and $6.27 \times 10^{22} \text{ cm}^{-3}$, respectively.

A direct influence of lithium number density is seen in the plots of conductivity of Fig. 9. The conductivity increases with both Li/P ratio and nitrogen content; however, the degree of the increase from the non-nitrided composition varies significantly with the lithium content. If only $\text{LiPO}_{1.5}\text{N}$ is formed, the much greater n_{Li^+} increases the conductivity most at the highest nitrogen content, but the dielectric constant of the nitride network also contributes to this improvement. On the other hand, the difference between the number density of ions of $\text{Li}_2\text{PO}_2\text{N}$ and Li_3PO_4 is less significant, which, added to the fact that nitridation of the orthophosphate does not result in pure $\text{Li}_2\text{PO}_2\text{N}$ but also some Li_2O , contributes to a much smaller increase of conductivity with respect to that obtained on nitridation of LiPO_3 . Nevertheless, the stronger influence of the higher dielectric constant in $\text{Li}_2\text{PO}_2\text{N}$ still contributes to some positive change in conductivity with respect to Li_3PO_4 .

3.4. Structural considerations of the modelled materials

Regarding the manner in which the oxynitride amorphous network could influence ionic conduction, some further structural aspects must be considered. In view of the calculated ionic conductivity along with the Li/P ratio and incorporated nitrogen, we have demonstrated that the mobility of Li^+ ions will be inherently dependent on their density, as well as on the increased dielectric constant of the resultant oxynitride amorphous network, whether in the form of a glass or an amorphous film. The network structure can thus be represented in terms of the different tetrahedra representing phosphate and nitrided

phosphate units of the chemical groupings, on which the thermodynamic model of associated solutions is based. These building units are the three types of $[\text{PO}_4]$ tetrahedra under different degrees of bonding with their neighbours, PO_3^{3-} , $\text{P}_2\text{O}_7^{4-}$ and PO_4^{3-} , and the $[\text{PO}_2\text{N}_2]$ tetrahedra that constitute the backbone of the oxynitride phases, $\text{Li}_2\text{PO}_2\text{N}$ and the new phase, herein proposed as $\text{LiPO}_{1.5}\text{N}$. This last phase is expected for oxynitrides near the LiPO_3 composition, as shown above, so the glass network of oxynitride compositions from a lithium metaphosphate glass are composed of the combination of $[\text{PO}_4]$ and $[\text{PO}_2\text{N}_2]$ tetrahedra. This hypothesis is very much supported by previous reports of lithium oxynitride phosphate glasses. Their structure has been shown to strongly depend on the type of glass-modifier elements in their composition. Muñoz showed that the types of tetrahedral units of the oxynitride network, $[\text{PO}_3\text{N}]$ and $[\text{PO}_2\text{N}_2]$ groups that are obtained by the oxygen-for-nitrogen substitution are present in different proportions when comparing NaPON and LiPON metaphosphate glasses.¹² In the former, there is a preponderance of $[\text{PO}_3\text{N}]$ over $[\text{PO}_2\text{N}_2]$ units, which do not appear in significant proportions until high nitrogen contents, while in the latter, $[\text{PO}_2\text{N}_2]$ units represent the great majority at both low and high nitrogen contents. The reaction of nitridation in a lithium metaphosphate glass can then be represented by the set of reactions of formation of LiPO_3 , from Li_2O and P_2O_5 , and $\text{LiPO}_{1.5}\text{N}$, as indicated by the thermodynamic modelling presented earlier and from which a structure composed of $[\text{PO}_4]$ and $[\text{PO}_2\text{N}_2]$ units arises. If a small amount of $[\text{PO}_3\text{N}]$ groups appear in the oxynitride glasses obtained by ammonolysis, it is only because, in the course of nitridation, metastable groupings may form that are frozen in once the reaction is stopped and which ultimately form the structural units of the system in equilibrium. It is proposed here that oxynitride glasses derived from NaPO_3 would be composed of the sum of $[\text{PO}_4]$ and $[\text{PO}_3\text{N}]$ tetrahedral units that would originate a new sodium oxynitride phosphate, which to date has not been obtained. In fact, the oxynitride $\text{Na}_2\text{Mg}_2\text{P}_3\text{O}_9\text{N}$ is a known crystalline oxynitride whose structure is based on $[\text{PO}_3\text{N}]$ tetrahedra linked by triply coordinated nitrogen atoms.⁴¹

3.5. Further implications of the thermodynamic approach to calculate ionic conductivity

Because of the experimental inconveniences to normalise the chemical composition of amorphous electrolytes, most particularly of those obtained *via* deposition by magnetron sputtering, neither the relevant experimental parameters to be considered in exploring a standardised conduction mechanism nor, more importantly, a way to predict the ionic conductivity for designing new electrolyte compositions can be easily found in the literature. Regardless of the method of synthesis of the LiPON electrolytes, the procedure presented here is a general means for the prediction of conductivity in terms of the chemical composition. Since the methodology can be of general application, it may also be extrapolated to the prediction of material properties of other chemistries. In fact, if the system of composition under study is based on oxides, and no oxynitride



phases are to be considered, the solution to the problem can be even simpler, since, if all oxide components of the equilibrium phase diagram of the system are known, then, there is no need for estimation of new Gibbs energy functions. The method that we have developed here for the LiPON electrolytes may thus predict the ionic conductivity of any type of amorphous solid electrolyte material. Furthermore, because no adjustable parameters are considered, the method allows us to obtain a model of the ionic conductivity for any range of composition of interest. In turn, research may be focused on adapting the synthesis method to achieve the highest conductivity, which represents a great advantage compared to a trial-and-error approach considering many compositions and experimental procedures.

4. Conclusions

The application of the model of associated solutions is suitable for the calculation of the conduction properties of LiPON compositions for any lithium and nitrogen content in both glasses and amorphous thin films. As a result of the theoretical derivation of the Gibbs formation energies developed for the two oxynitride compounds, we now have a powerful tool for prediction of the properties of amorphous solid electrolytes, in the form of bulk glasses or films. The existence of a new oxynitride, $\text{LiPO}_{1.5}\text{N}$, is proposed, based on the results of nitridation of lithium pyrophosphate. This phase also forms from the nitridation of lithium metaphosphate. The structure of this new compound consists of $[\text{PO}_2\text{N}_2]$ tetrahedral units, as is the case in the known phase of $\text{Li}_2\text{PO}_2\text{N}$. However, no other oxynitride is expected to appear after oxygen-for-nitrogen substitution from Li_3PO_4 . These results validate the scheme of reactions of formation of oxynitride compounds. Throughout the quantification of the molar amount of phosphate and oxynitride phosphate compounds at each composition, the number density of lithium ions that take part in ionic conduction of the modelled solids may be calculated. The conductivity increases monotonously with the lithium content from metaphosphate to orthophosphate compositions. Although the introduction of nitrogen increases conductivity, the magnitude of the increase reduces for the highest lithium contents. The greatest increase in conductivity after nitridation was obtained in the metaphosphate composition, in correspondence with published experimental data for LiPON glasses. Furthermore, the values of $\log_{10} \sigma$ and E_a obtained by the model presented in this work are very close to experimental values for LiPON thin films.

Author contributions

A. López-Grande: conceptualization, data curation, formal analysis, investigation, software, visualization, writing original draft, writing – review & editing; G. C. Mather: data curation, formal analysis, investigation, methodology, software, validation, visualization, writing – review & editing; F. Muñoz: conceptualization, data curation, formal analysis, funding acquisition, investigation, methodology, project administration, methodology, project administration, resources,

supervision, validation, visualization, writing original draft, writing – review & editing.

Conflicts of interest

The authors do not have any conflict of interest to declare.

Acknowledgements

The authors thank funding from projects LUMGLASS (PID2020-115419GB-C21/AEI/10.13039/501100011033) and FUNGLASS (European Union Horizon 2020 research and innovation program under grant agreement No 739566). We acknowledge support of the publication fee by the CSIC Open Access Publication Support Initiative through its Unit of Information Resources for Research (URICI).

References

- M. J. Wang, E. Carmona, A. Gupta, P. Albertus and J. Sakamoto, *Nat. Commun.*, 2020, **11**, 5201.
- D. Xiaoa, J. Tonga, Y. Fenga, G. Zhonga, W. Lia and C. Yanga, *Solid State Ionics*, 2018, **324**, 202.
- J. B. Bates, N. J. Dudney, G. R. Gruzalski, R. A. Zuhr, A. Choudhury and C. F. Luck, *Solid State Ionics*, 1992, **53–56**, 647–654.
- Y. H. Jouybari, F. Berkemeier, A. Schäfer and G. Schmitz, *J. Power Sources*, 2018, **394**, 160–169.
- B. Wang, B. S. Kwak, B. C. Sales and J. B. Bates, *J. Non-Cryst. Solids*, 1995, **183**, 297.
- B. Carrette, M. Ribes and J. L. Souquet, *Solid State Ionics*, 1983, **9–10**, 735–737.
- A. Magistris, G. Chiodelli and M. Duclot, *Solid State Ionics*, 1983, **9–10**, 611–615.
- M. Tatsumisago, K. Yoneda, N. Machida and T. Hinami, *J. Non-Cryst. Solids*, 1987, **95–96**, 857.
- Z. Hu, D. Li and K. Xie, *Bull. Mater. Sci.*, 2008, **31**, 681.
- V. Lacivita, A. S. Westover, A. Kercher, N. D. Phillip, G. Yang, G. Veith, G. Ceder and N. J. Dudney, *J. Am. Chem. Soc.*, 2018, **140**, 11029.
- V. Lacivita, N. Artrith and G. Ceder, *Chem. Mater.*, 2018, **30**, 7077.
- F. Muñoz, *Pure Appl. Chem.*, 2022, **94**, 189.
- J. B. Bates, N. J. Dudney, G. R. Gruzalski, R. A. Zuhr, A. Choudhury and C. F. Luck, *J. Power Sources*, 1993, **43–44**, 103.
- P. Hockicko, P. Bury and F. Muñoz, *J. Non-Cryst. Solids*, 2013, **363**, 140.
- N. Mascaraque, J. L. G. Fierro, A. Durán and F. Muñoz, *Solid State Ionics*, 2013, **233**, 73.
- F. Muñoz, A. Durán, L. Pascual, L. Montagne, B. Revel and A. C. M. Rodrigues, *Solid State Ionics*, 2008, **179**, 574.
- A. López-Grande, R. Dagupati, P. Galán del Sastre and F. Muñoz, *J. Am. Ceram. Soc.*, 2021, **104**, 5625.
- B. A. Shakhmatkin, N. M. Vedishcheva, M. M. Shultz and A. C. Wright, *J. Non-Cryst. Solids*, 1994, **177**, 249.



- 19 O. L. Anderson and D. A. Stuart, *J. Am. Ceram. Soc.*, 1954, **37**, 573.
- 20 K. Senevirathne, C. S. Day, M. D. Gross, A. Lachgar and N. A. W. Holzwarth, *Solid State Ionics*, 2013, **233**, 95.
- 21 F. Tessier and A. Navrotsky, *Chem. Mater.*, 2000, **12**, 148.
- 22 B. De B. Darwent, *Natl. Stand. Ref. Data Ser.*, 1970, **31**, 52.
- 23 W. M. Latimer, *J. Am. Chem. Soc.*, 1951, **73**, 1480.
- 24 W. M. Latimer, *J. Am. Chem. Soc.*, 1921, **43**, 818.
- 25 J. Richter and W. Vreuls, *Ber. Bunsen. Phys. Chem.*, 1979, **83**, 1023.
- 26 W. M. Haynes and D. R. Lide, *Handbook of Chemistry and Physics*, 91st edn, 2010, ISBN 978-1-4398-2077-3.
- 27 J.-L. Souquet, M. L. F. Nascimento and A. C. M. Rodrigues, *J. Chem. Phys.*, 2010, **132**, 034704.
- 28 P. Hockicko, P. Bury and F. Muñoz, *Commun. – Sci. Lett. Univ. Zilina*, 2013, **15**, 33.
- 29 B. Elouadi, M. Ouchetto, E. H. Arbib and N. Amraoui, *Phase Trans.: A Multinatl. J.*, 1988, **13**, 219.
- 30 S. V. J. Kenmuir, PhD Thesis, Durham University 1986.
- 31 J.-C. Guitel and I. Tordjman, *Acta Cryst.*, 1976, **B32**, 2960.
- 32 A. Daidouh, M. L. Veiga, C. Pico and M. Martinez-Ripoll, *Acta Cryst.*, 1997, **C53**, 167.
- 33 A. S. Korotkov and V. V. Atuchin, *Optics Commun.*, 2008, **281**, 2132.
- 34 M. A. T. Marple, T. A. Wynn, D. Cheng, R. Shimizu, H. E. Mason and Y. S. Meng, *Angew. Chem., Int. Ed.*, 2020, **59**, 22185.
- 35 D. Massiot, F. Fayon, M. Capron, I. King, S. Le Calvé, B. Alonso, et al., *Magn. Reson. Chem.*, 2002, **40**, 70.
- 36 V. I. Voronin, E. A. Sherstobitova, V. A. Blatov and G. h. Shekhtman, *J. Solid State Chem.*, 2014, **211**, 170.
- 37 Y.-W. Hu, I. D. Raistrick and R. A. Huggins, *J. Electrochem. Soc.*, 1977, **124**, 1240.
- 38 R. A. Huggins, *Electrochim. Acta*, 1977, **22**, 773.
- 39 R. Marchand, L. Agliz, R. Boukbir and A. Quemerais, *J. Non-Cryst. Solids*, 1988, **103**, 35.
- 40 T. M. Alam, S. Conzone, R. K. Brow and T. J. Boyle, *J. Non-Cryst. Solids*, 1999, **258**, 140.
- 41 D. Massiot, R. Conanec, W. Feldmann, R. Marchand and Y. Laurent, *Inorg. Chem.*, 1996, **35**, 4957.

